Direct Numerical Simulation of Self-Propelled Swimming of 3D Bionic Fish School †

Chui-Jie WU[1] ‡ & Liang WANG[2]

1. State Key Laboratory of Structural Analysis for Industrial Equipment, Dalian University of Technology, Dalian 116024

2. Research Center for Fluid Dynamics, PLA University of Science and Technology, Nanjing 211101

ABSTRACT

Direct numerical simulation of self-propelled swimming of three dimensional bionic fish and fish school in a viscous flow in a tank are investigated. The swimming rule and the profile of 3D fish from previous experimental measurements of living fish are used in the study. A parallel software package for the 3D moving boundary problem is obtained, which combines the adaptive multi-grid finite volume method and the methods of immersed boundary and VOF (Volume of Fluid). With the CFD package the results of the self-propelled swimming and control of a 3D bionic fish and fish school in a viscous fluid is obtained.

Key words: Adaptive multi-grid, Immersed boundary method, Self-propelled swimming, Fish school, 3D bionic fish

1. Introduction

The mechanics of fish swimming is an attractive topic fluid mechanics, and due to uncontrollable of fish, numerical simulation becomes one of the major tools in the study. But up to now, there is no report about the numerical simulations of three-dimensional self-propelled swimming of fish in a viscous fluid, let alone the control of fish.

In this paper, first, a parallel software package for the 2D and 3D moving boundary problem is obtained, which combines the adaptive multi-grid finite volume method and the methods of immersed boundary and VOF (Volume of Fluid). The reliability of the algorithm and code is verified with the numerical results of flow around a 2D circular cylinder. Then, three dimensional numerical simulations of self-propelled swimming of bionic fish and fish school in a viscous flow in a tank are investigated.

2. Basic equations and numerical algorithm

2.1 Basic equations

In the process of numerical simulation of the self-propelled swimming of a 3D bionic fish, the basic equations solved are the 3D incompressible continuity equation and Navier-Stokes equations.

$$\nabla \cdot \boldsymbol{u} = 0, \tag{2.1}$$

$$\frac{\partial \boldsymbol{u}}{\partial t} + (\boldsymbol{u} \cdot \nabla)\boldsymbol{u} = -\nabla \left(\frac{p}{\rho} + gz \right) + \nu \nabla^2 \boldsymbol{u}. \tag{2.2}$$

where, $\boldsymbol{u}$, p, ρ, g and $\nu = \mu/\rho$ are velocity, pressure, density, gravitational acceleration and the kinematics viscosity, respectively.

2.2 Numerical algorithm

The finite volume method is used to solve the set of equations of the continuity equation and three-dimensional incompressible Navier-Stokes equations. The adaptive grid technique is used in the computation,

† Project supported by the National Science Foundation of China (#10172095 and #10672183)

‡ Email: cjwudut@dlut.edu.cn or chuijie.wu@gmail.com

and the domain is spatially discreted using cubic finite volumes organised hierarchically as an octree. The projection method and multi-grid method are used to solve the pressure Poisson equation. The convective term is discreted with second order upwind schemes[1], and the VOF(Volume Of Fluid) method is applied to treat free surface boundaries. Next, we describe the algorithm according to [4].

2.2.1 Time discretization: the fractional-step projection method

The time discretization uses the fractional-step projection method. First, following equation is used to get the temporary values of velocity $\boldsymbol{U}^{**}$:

$$\frac{\boldsymbol{U}^{**}-\boldsymbol{U}^{n}}{\Delta t}=\left[-(\boldsymbol{U}\cdot\nabla)\boldsymbol{U}+\nu\nabla^{2}\boldsymbol{U}\right]^{n+1/2} \tag{2.3}$$

Then, apply the project operator to $\boldsymbol{U}^{**}$ to obtain the new velocity field $\boldsymbol{U}^{n+1}$ and fractional-step pressure $p^{n+1/2}$. The projection method depends on the Hodge decomposition of velocity field:

$$\boldsymbol{U}^{**}=\boldsymbol{U}+\nabla\phi \tag{2.4}$$

where, $\boldsymbol{U}$ is $\nabla\cdot\boldsymbol{U}=0$ in the computation domain Ω, and on the boundary, $\partial\Omega$ meets $\boldsymbol{U}\cdot\boldsymbol{n}=0$. To apply the divergence to the both sides of equation(2.4) to get the following Poisson equation,

$$\nabla^{2}\phi=\nabla\cdot\boldsymbol{U}^{**} \tag{2.5}$$

and its boundary conditions are

$$\frac{\partial\phi}{\partial\boldsymbol{n}}=\boldsymbol{U}^{**}\cdot\boldsymbol{n},\qquad on\ \ \partial\Omega \tag{2.6}$$

Therefore the divergence-free velocity field is defined as

$$\boldsymbol{U}=\boldsymbol{U}^{**}-\nabla\phi \tag{2.7}$$

This equation defines a projection from $\boldsymbol{U}^{**}$ to the divergence-free velocity field $\boldsymbol{U}$, where ϕ can be obtained by solving Poisson equation (2.5).

2.2.2 Spatial discretization: the finite volume cells in an octree

The domain is spatially discreted using cubic finite volumes organised hierarchically as an octree. A 2D example of spatial discretization and the corresponding tree representation is given in Fig. (2.1). The length of a finite volume(cell) edge is denoted by h. Each cell may be the parent of up to eight children. The root cell is the base of the tree and a leaf cell is a cell without any child. The level of a cell is defined by starting from zero for the root cell and by adding one every time a group of four descendant children is added. Each cell $\mathcal{C}$ has a direct neighbour at the same level in each direction d, noted $\mathcal{N}_d$. Each of these neighbours is accessed through a face of the cell, noted $\mathcal{C}_d$. In order to handle embedded solid boundaries, we also define mixed cells which are cut by a solid boundary. The primitive variables of the N-S equations (velocity $\boldsymbol{U}$ and pressure P) are all defined at the centre of the cells.

To simplify the calculations at the cell boundaries, we add the constraints illustrated in Fig. (2.2): the levels of direct neighbouring cells cannot differ by more than one; the levels of diagonally neighbouring cells can not differ by more than one; all the cells directly neighbouring a mixed cell must be at the same level. The refinement necessary to conform to the constraint is indicated by the dotted lines in the figure.

The choice of a data structure to represent the tree is conditioned by: (a) for any given cell, efficient access to neighbouring cells and to cell level and spatial coordinates; (b) efficient traversal of all leaf cells, all cells at a given level and all mixed cells. We use the fully threaded tree structure presented by Khokhlov[3] which allows (a) to be performed in $\mathcal{O}(1)$ operations (versus $\mathcal{O}(\log N)$), and operations (b) are performed in $\mathcal{O}(N\log N)$, using the standard pointer-based tree description (N is the number of cells traversed).

2.3 Moving boundary with immersed boundary method and VOF method

In CFD, usually complex solid boundaries are treated with body-fit structural or nonstructural grids, and in such grids, the boundary conditions can be easily and accurately met. But the grid generation is a

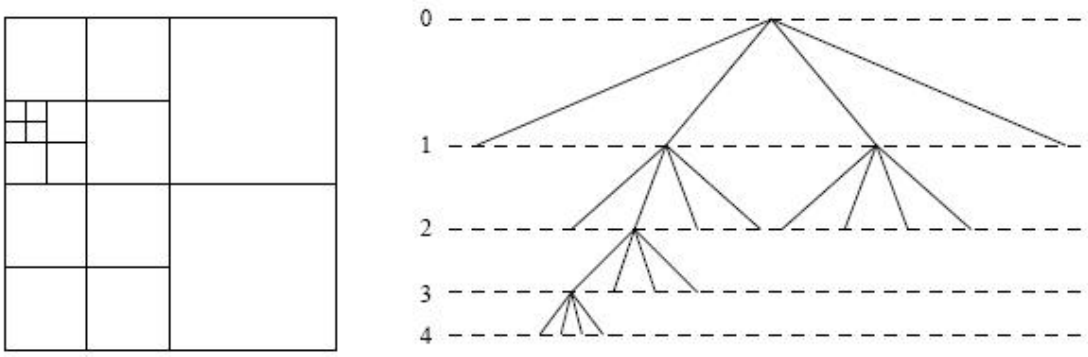

Fig. 2.1 Example of quadtree discretization and corresponding tree representation.

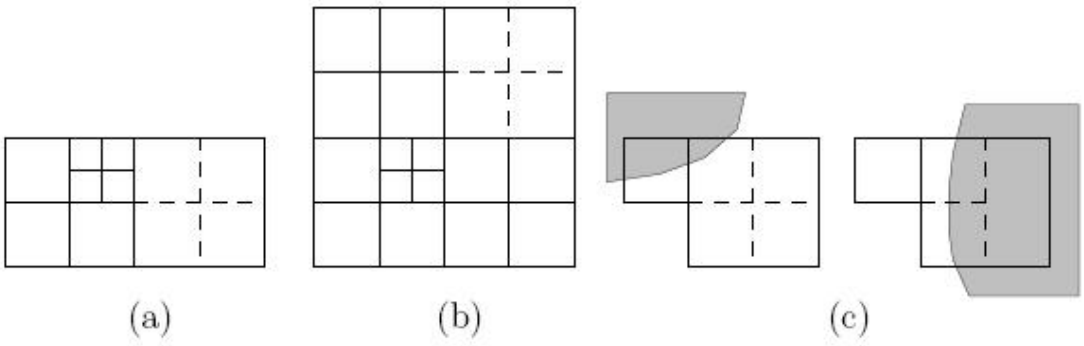

Fig. 2.2 Additional constraints on the quadtree discretization.

difficult and time consuming job. In this paper, the complex moving boundaries are treated with an immersed boundary method in the way of ghost-cell discrete force field[11].

The adaptive refinement strategy includes two steps. In the first step, all the leaf cells which satisfy a given criterion are refined. In a second step, we consider the parent cells of all the leaf cells, All of these cells which do not satisfy the refinement criterion are coarsened.

The following criterion is based on the norm of the local vorticity vector

$$\frac{h \parallel \bigtriangledown \times \boldsymbol{u} \parallel}{\max \parallel \boldsymbol{u} \parallel} > \tau \tag{2.8}$$

where, h is the minimum width of grids, $0 < \tau < 1$ is the threshold value of refinement. If the refinement criterion is only based on the norm of the local vorticity vector, the ghost cell is the finest cell can not be assured. Therefore, we introduce the mixed refinement criterion:

$$\max\left(\frac{h \parallel \nabla \boldsymbol{T} \parallel}{\max \parallel \boldsymbol{T} \parallel}, \quad \frac{h \parallel \nabla \times \boldsymbol{u} \parallel}{\max \parallel \boldsymbol{u} \parallel}\right) \quad > \quad \tau \tag{2.9}$$

where, T is a tracer of VOF(Volume of Fluid). If the closed regiom surrounded by the moving boundary is Ω, then

$$T \begin{cases} = 0, & \text{in } \Omega \\ \in (0,1), & \text{on } \partial\Omega \\ = 1, & \text{out side of } \Omega \end{cases} \tag{2.10}$$

VOF method is an effective method which can treat complicated free surface, proposed by Hirt and Nichols in 1975. The basic idea of this method is [2]: define functions a and $1-a$, which represent the relative fractional volume of water and air in the computational domain, respectively. In each cell, the sum of the fractional volume of water and air is equal to 1. For a computational cell, there are three cases:

(1) $a = 1$, which means that the cell is full of water;

(2) $a = 0$, which means that the cell is full of air;

(3) $0 < a < 1$, which means that the cell is partially occupied by water and the rest is occupied by air, that is there is an interface of water and air in the cell, i.e., a free surface.

The gradient of the fractional volume of water is used to determine the normal direction of free surface. After getting the values of VOF and gradient of each cell, the approximate position of the free surface in each cell can be obtained. The advantage of VOF method is that only one function is used to describe the various changes of free surface. Therefore, VOF method is one of the ideal methods applied in computational fluid dynamics when dealing with the problems of free surface.

The verification and validation of the numerical algorithm and the code can be find in [4].

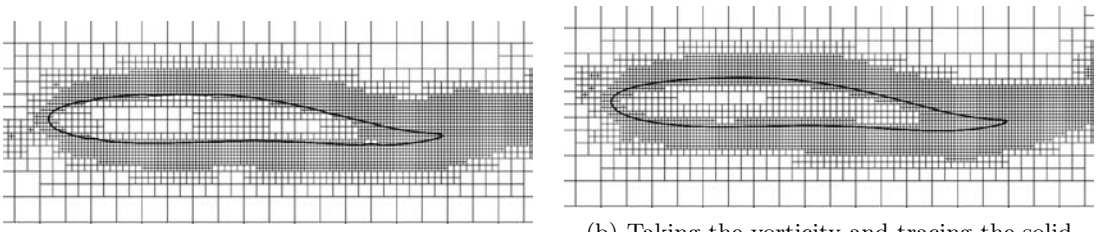

(a) Using the vorticity as the adaptive criteria

(b) Taking the vorticity and tracing the solid boundary together as the adaptive criteria

Fig. 2.3 The grids with different adaptive refinement conditions

In this study, the idea of VOF method is used to identify the interface of fluid and immersed boundary, thus the gradient of T can be used in the process of refinement of local grids. Fig.2.3(a) is the adaptive grids with vorticity as the adaptive criteria. From the figure it is seen that some part on the boundary the grids are coarser, which causes the depicting accuracy decrease on the body surface of bionic fish. But in Fig.2.3(b), the grids is obtained using the vorticity and ∇T together as the adaptive criteria. One can see that the grids intersected with the immersed boundary are all the finest, thus ensure the accurate represent of the moving boundary in the adaptive grids. The computational results shown in the paper are all using the relative value of total vorticity and the gradient of volume fraction together as the adaptive criteria, which meets the local condition of (2.9).

2.4 Validation test of the method

It is well known that the simulation with moving boundaries is very difficult to be verified, because experimental study of such flow is rarely. Therefore, the validation of the method is performed by simulating the flow past a circular cylinder immersed in an unbounded uniform flow. This flow has been studied quite extensively and a number of numerical and experimental data sets exist for it.

The simulations have been performed in a domain of of $16D \times 64D$ which large enough to minimize the effect of the outer boundary on the development of the wake. The Reynolds number is defined as $Re_D = u_\infty D/\nu$, where D is the cylinder diameter. Simulations have been performed at $Re_D = 100$ and results are compared with established experimental and numerical results.

We computed the results for $n = 6, 7, 8$, respectively, with the technique of multi-objective in the adaptive refinement. The adaptive grids are shown in Fig.2.4. From the figure it is shown that the grids intersected with the immersed boundary are all finest grids. From the figure it is seen that when the level of grid is equal to 8, the centers of elements intersected with the immersed boundary are all most coincided with the immersed

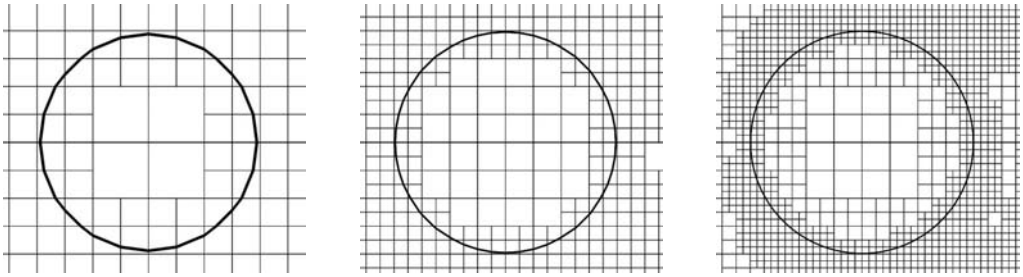

(a) Level 6 (b) Level 7 (c) Level 8

Fig. 2.4 The adaptive boundary grids of circular cylinder

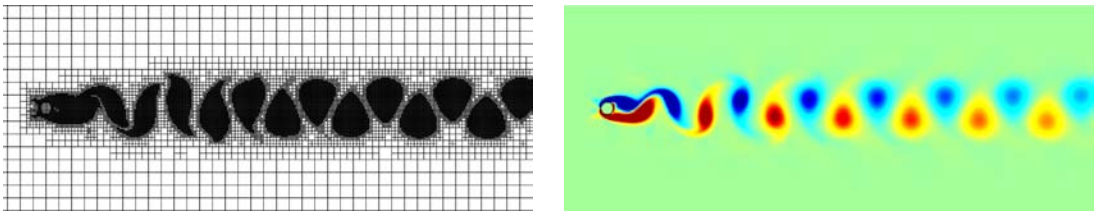

(a) The adaptive grids (b) The vorticity field

Fig. 2.5 Vorticity contour and corresponding adaptive grid of the flow past a circular cylinder at $Re_D = 100$

boundary. Fig.2.5 shows the adaptive grids and the corresponding vorticity field, which are agreed very well. From the results shown in Fig.2.4 and Fig.2.5, we can conclude that the adaptive method of multi-objective is effective.

	$St = fD/u_\infty$	$C_d = F_d/(0.5\rho u_\infty^2 D)$
Current study (28 IB points around the cylinder)	0.157	1.415
Current study (60 IB points around the cylinder)	0.166	1.355
Current study (124 IB points around the cylinder)	0.171	1.371
Tseng and Ferziger [11]	0.164	1.42
Lai and Peskin [10]	0.165	1.4473
Dias and Majumdar [6]	0.171	1.395
Kim et al.[9]	0.165	1.33
Zdravkovich(Exp. as reported in [13])	0.165	1.40

表 2.1 Comparison of several results for cylinder flow at $Re_D = 100$

For flow over the cylinder at $Re_D = 100$, Table 2.1 compares the results obtained by this numerical algorithm and those from an experiment and other numerical simulations, indicating that our result is reasonably good. From Fig. 2.5, it can be seen that the position of vortex core is corresponding to the zone with the finest grid. Therefore, adaptive refinement strategy is validated.

3. The motion equation and the body and swing parameters of a 3D bionic fish

3.1 Governing equations

The governing equations for the fluid motion are (2.2). The governing equations for the self-propelled bionic fish are

$$m\frac{\mathrm{d}\boldsymbol{u}}{\mathrm{d}t} = \boldsymbol{F}, \quad \frac{\mathrm{d}\boldsymbol{L}}{\mathrm{d}t} = \boldsymbol{M} \tag{3.1}$$

where, m is the mass of bionic fish; $\boldsymbol{u}$ is the velocity vector; $\boldsymbol{F}$ is the hydrodynamic force; $\boldsymbol{M}$ is the moment and $\boldsymbol{L}$ is the moment of momentum

$$\boldsymbol{L} = \sum_i m_i \boldsymbol{r}_i \times \boldsymbol{v}_i \tag{3.2}$$

where, m_i is the mass of segment i, $\boldsymbol{r}_i$ is the gravity center of segment i, as shown in Fig.3.1. $\boldsymbol{v}_i$ is its rate of change of position in the local coordinate. $\boldsymbol{v}_i$ include two parts, i.e.,

$$\boldsymbol{v}_i = \boldsymbol{v}_{fi} + \boldsymbol{\omega}_i \times \boldsymbol{r}_i \tag{3.3}$$

where, $\boldsymbol{v}_{fi}$ is the part determined by the given flapping rule. $\boldsymbol{\omega}_i$ is the angular speed of segment i. Hence,

$$\boldsymbol{L} = \sum_i m_i \boldsymbol{r}_i \times \boldsymbol{v}_{fi} + \sum_i m_i r_i^2 \boldsymbol{\omega}_i \tag{3.4}$$

If we want to get the unique solution of the equations of the moment of momentum in (3.1), the sufficient and necessary condition is

$$\boldsymbol{\omega}_1 = \boldsymbol{\omega}_2 = \cdots = \boldsymbol{\omega} \tag{3.5}$$

Therefore,

$$m\frac{\mathrm{d}\boldsymbol{u}}{\mathrm{d}t} = \boldsymbol{F}, \quad \frac{\mathrm{d}}{\mathrm{d}t}\left(\sum_i m_i \boldsymbol{r}_i \times \boldsymbol{v}_{fi}\right) + \frac{\mathrm{d}}{\mathrm{d}t}\left(\boldsymbol{\omega}\sum_i m_i r_i^2\right) = \boldsymbol{M} \tag{3.6}$$

After got $\boldsymbol{u}$ and $\boldsymbol{\omega}$, the new position coordinate and new angle of attack of fish body can be found by

$$\frac{\mathrm{d}\boldsymbol{x}}{\mathrm{d}t} = \boldsymbol{u}, \quad \frac{\mathrm{d}\boldsymbol{\theta}}{\mathrm{d}t} = \boldsymbol{\omega} \tag{3.7}$$

where, $\boldsymbol{\theta} = \theta_x \boldsymbol{i} + \theta_y \boldsymbol{j} + \theta_z \boldsymbol{k}$, and θ_x, θ_y and θ_z are the angles of the projection of the central line of the body of fish on the plans of $y-z$, $z-x$ and $x-y$ to the positive directions of y, z and x axis, respectively.

3.2 Local and global coordinates

In the computation, we use the unit time t and the length of bionic fish L to do the nondimensionalization. In the study of self propel process of the bionic fish, two sets of coordinates are used, as shown in Fig.3.1. One is the global experiment coordinate (x, y, z), which enables the position of the fish's centre of mass to be defined as (x_0, y_0, z_0). The other is the local coordinate settled on the center of weight of fish (x_l,y_l,z_l), which is called as the fish body coordinate. The final link between these two coordinate systems is the angle θ, shown in Fig.3.1, which defines the orientation of x_l (the generatrix) relative to the x direction in the global coordinates.

From (3.13) one can see that in the flapping process, every point on the central line is symmetry about x_l, which is called as the central line of flap. In the self-propelled swimming of a 2D bionic fish, under the influence of total moment, between the axis x_l of fish body coordinate and the axis x under the experiment coordinate, there will generate an angle θ, which is called the angle of attack of fish body, as shown in Fig.3.1. For a 3D bionic fish, the angle of attack of fish body has three components, which are the angles between the projection of the central line to the three plans in the coordinate of experiment and the positive direction of axis, respectively.

The coordinate of fish body and the coordinate of experiment are connected by the weight center of fish and the angle of attack of fish body. For example, assume that at some time in the coordinate of experiment

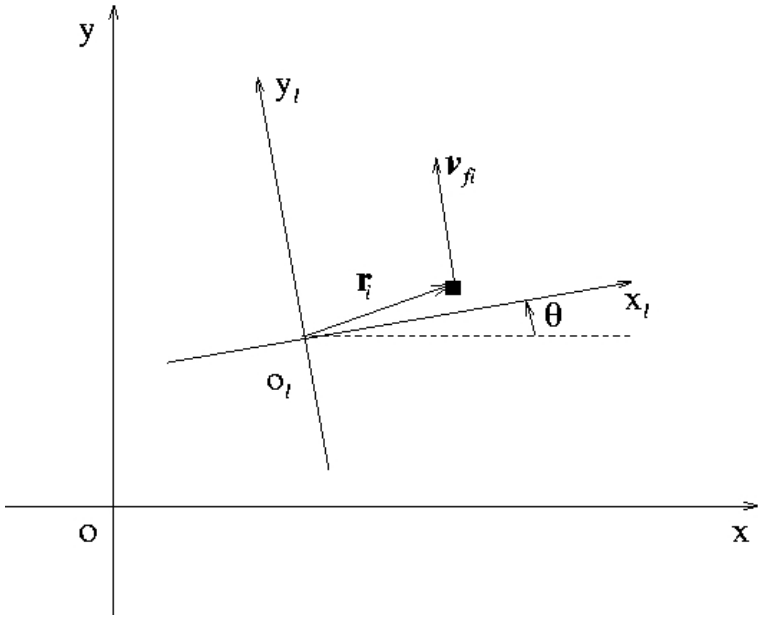

Fig. 3.1 The fish body coordinate and the experiment coordinate

the weight center of a 2D bionic fish is (x_0, y_0), the angle of attack of fish body is θ, then in the coordinate of experiment, an arbitrary point (x_l, y_l) on the body of the bionic fish in the coordinate of fish body is

$$x = x_0 + x_l\cos(\theta) - y_l\sin(\theta), \quad y = y_0 + x_l\sin(\theta) + y_l\cos(\theta) \tag{3.8}$$

where, x_0, y_0, θ are all the function of time, which is obtained by solving the control equation of motion of the bionic fish.

From above analysis, we find that the point of weight of the fish is the key which links two coordinates together. (3.9) shows the coordinate of weight of 2D bionic fish in the flapping process under the coordinate of body of fish.

$$x_{l0} = \frac{1}{m}\iint_D x_l\rho(x_l, y_l)\mathrm{d}\sigma, \quad y_{l0} = \frac{1}{m}\iint_D y_l\rho(x_l, y_l)\mathrm{d}\sigma \tag{3.9}$$

where, m is the mass of the bionic fish, (x_l, y_l) is the coordinate of the weight of the arbitrarily mass unit in the body of the bionic fish, and $\rho(x_l, y_l)$ is the density of this point. We assume the density of the bionic fish is identical to that of water.

3.3 Fish geometries and flapping rule

3.3.1 Fish geometries

In the present work, we employ body shapes representing a RoboTuna[14] to study the self-propelled swimming of bionic fish school.

In [14], the profile of the body is given as

$$\begin{cases} z_l(x_l) = \pm 0.152\tanh\left(6x_l + 1.8\right), & -0.3 \leqslant x_l \leqslant 0.1 \\ z_l(x_l) = \pm\left[0.075 - 0.076\tanh\left(7x_l - 3.15\right)\right], & 0.1 < x_l \leqslant 0.7 \end{cases} \tag{3.10}$$

At each horizontal position x_l, the body sections are assumed to be elliptical with a major to minor ratio of $AR = 1.5$, where the major axis corresponds to the height of the body. The profile is shown as Fig.3.2(a). Since the height of the caudal peduncle is too small to be distinguished by the immersed boundary method. Therefore, the rear part($x_l > 0.35$) of the profile is fitted again. The new profile of the body is given as

$$\begin{cases} z_l(x_l) = \pm 0.152 \tanh\left(6x_l + 1.8\right), & -0.3 \leqslant x_l \leqslant 0.1 \\ z_l(x_l) = \pm\left[0.075 - 0.076 \tanh\left(7x_l - 3.15\right)\right], & 0.1 < x_l \leqslant 0.35 \\ z_l(x_l) = \pm[1.749 \tanh(x_l) - 3.331 \tanh(2x_l) + 1.976 \tanh(3x_l)], & \\ & 0.35 < x_l \leqslant 0.7 \end{cases} \tag{3.11}$$

The new profile is shown in Fig.3.2(b).

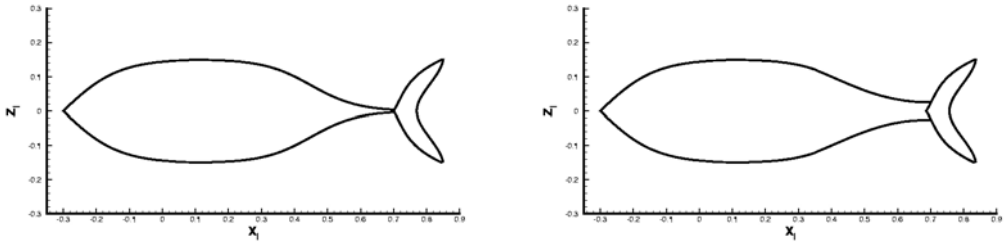

(a) original profile (b) new profile

Fig. 3.2 The original and new profiles of fish body and caudal fin

As shown in Fig.3.2, the leading edge and trailing edge profiles are given by

$$\begin{cases} z_l(x_l)_{LE} = 39.543\left|z_l\right|^3 - 3.685\left(z_l\right)^2 + 0.636\left|z_l\right| + 0.7, & -0.15 \leqslant z_l \leqslant 0.15 \\ z_l(x_l)_{TE} = -40.74\left|z_l\right|^3 + 9.666\left(z_l\right)^2 + 0.77, & -0.15 \leqslant z_l \leqslant 0.15 \end{cases} \tag{3.12}$$

For the same reason, the caudal fin has chord-wise sections of NACA 0040 shape, instead of NACA 0016 shape in [14]. The 3D profile of fish body with caudal fin is shown in Fig. default-profile3D.

3.3.2 Flapping rule

We assume that bending of the fish-like body happens only within the $x_l - y_l$ plan, and the tail is assumed to oscillate and rotate as a rigid body while the finlets and secondary fins follow the motion of the body([14]).

In the self-propelled swimming case, the motion of the body could be fully described by specifying the motion of its backbone with several key kinematic parameters. The motion is characterized by a travelling backbone wave of smoothly varying amplitude. In local coordinate system, The backbone waveform $y_l(x_l, t)$ can be written as

$$\begin{cases} y_l(x_l, t) = a(x_l)\sin(k_w x_l - \omega t) \\ a(x_l) = c_1 x_l + c_2 x_l^2, \quad -0.3 \leqslant x_l \leqslant 0.7 \end{cases} \tag{3.13}$$

where, $k_w = 2\pi/\lambda$ is the wavenumber, corresponding to wavelength λ, $\omega = 2\pi/T$ the circular frequency, corresponding to tail-beat period T, and$x_l = 0$ is located at a distance of the body length from the nose, with positive x in the direction from the nose to the tail. The amplitude envelope a(x) is defined with adjustable parameters c_1 and c_2,

The front point on the articulated caudal fin where it is attached to the caudal peduncle follows the path of the peduncle, and additionally the fin is allowed to undergo a pitch motion around this front point.

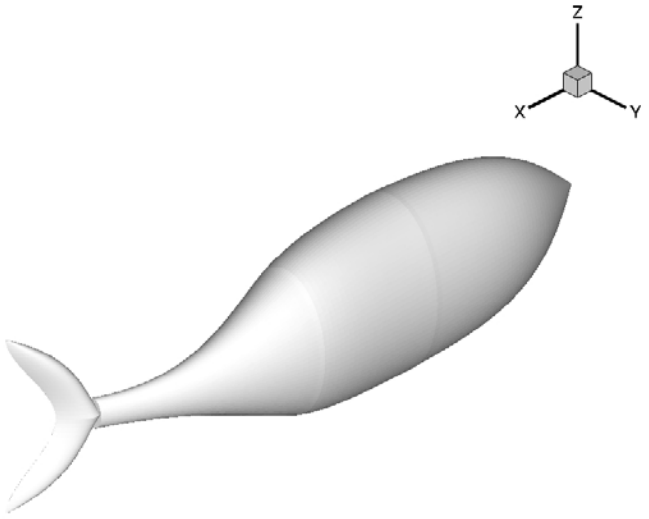

Fig. 3.3 3D profile of fish body with caudal fin

This pitch motion has the same frequency ω as the backbone wave-like motion while its temporal phase angle is behind that of the lateral motion of the front point by a phase difference ψ. At any time t, the angle of attack θ with respect to the x_l-axis is given by

$$\theta = \alpha \sin(k_w x_{lp} - \omega t + \psi) \tag{3.14}$$

where, α is the maximum angle of attack. $x_{lp} = 0.7$, is the x_l-coordinate of the peduncle.

In this study, the key kinematic parameters are taken as $T = 1.0$, $\lambda = 1.22$, $\alpha = 30^o$, $\psi = 90^o$, $c_1 = 0.0$, $c_2 = 0.155$.

3.4 Boundary and initial condition

3.4.1 Boundary condition of computational region and initial condition

The computational region has six boundaries, all of which are set to be no slip boundary conditions, i.e.

$$u_b = v_b = w_b = 0 \tag{3.15}$$

The initial condition is

$$u = v = w = 0 \tag{3.16}$$

3.4.2 Immersed boundary condition

After the shape of 3D bionic fish is fixed, the most important is to determine the velocity on the boundary, which is consisted by following three parts.

(1). Velocity $\boldsymbol{V}_0$ arose from the hydrodynamic force.

$$\boldsymbol{V}_0 = u_0\boldsymbol{i} + v_0\boldsymbol{j} + w_0\boldsymbol{k} \tag{3.17}$$

(2). Linear velocity $\boldsymbol{V}_r$ arose from rotation.

$$\boldsymbol{V}_r = \boldsymbol{\omega} \times (\boldsymbol{x} - \boldsymbol{x}_0) \tag{3.18}$$

where, $\boldsymbol{x}$ is one point on the surface, and $\boldsymbol{x}_0$ is the mass center.

(3) Velocity $\boldsymbol{V}_f$ arose from the flapping.

In the local coordinate system, the motion of fish body happens only within the $x_l - y_l$ plan. According to equation (3.13), the velocity of fish body is

$$\begin{cases} u_{lf} = w_{lf} = 0 & -0.3 \leqslant x_l \leqslant 0.7 \\ v_{lf} = \dot{y_l}(x_l, t) = -\omega a(x_l)\cos(k_w x_l - \omega t), & -0.3 \leqslant x_l \leqslant 0.7 \end{cases} \tag{3.19}$$

At any time t, the x_l-coordinate of the peduncle is

$$x_{lp} = 0.7, \quad y_{lp}(t) = a(x_{lp})\sin(k_w x_{lp} - \omega t) \tag{3.20}$$

Its velocity is

$$v_{lp} = \dot{y}_{lp}(t) = -\omega a(x_{lp})\cos(k_w x_{lp} - \omega t) \tag{3.21}$$

The angular velocity of caudal fin round the point (x_{lp}, y_{lp}) is

$$\omega_{lf} = -\omega\alpha\cos(k_w x_{lp} - \omega t + \psi) \tag{3.22}$$

Then, the linear velocity arose from the rotation is

$$\begin{cases} u_{lf} = -\omega_{lf}(y_l - y_{lp}), & x_l > 0.7 \\ v_{lf} = v_{lp} + \omega_{lf}(x_l - x_{lp}), & x_l > 0.7 \end{cases} \tag{3.23}$$

where, (x_l, y_l) is the point on the surface of caudal fin. Therefore, in the local coordinate system, the velocity arose from the flapping is

$$\begin{cases} u_{lf} = \begin{cases} 0, & -0.3 \leqslant x_l \leqslant 0.7 \\ -\omega_{lf}(y_l - y_{lp}), & x_l > 0.7 \end{cases} \\ v_{lf} = \begin{cases} -\omega a(x_l)\cos(k_w x_l - \omega t), & -0.3 \leqslant x_l \leqslant 0.7 \\ v_{lp} + \omega_{lf}(x_l - x_{lp}), & x_l > 0.7 \end{cases} \\ w_{lf} = 0 \end{cases} \tag{3.24}$$

Using the angle θ, $\boldsymbol{V}_{lf}$ can be transform to $\boldsymbol{V}_f$ which is the corresponding velocity in the global coordinate system.

In result, the boundary velocity $\boldsymbol{V}_b$ on the surface of fish is

$$\begin{cases} u_b = u_0 + u_r + u_f \\ v_b = v_0 + v_r + v_f \\ w_b = w_0 + w_r + w_f \end{cases} \tag{3.25}$$

3.5 Steps of a fully explicit scheme

We consider the self-propelled swimming along $-x$-direction. The computational domain is $[x_s, x_e] \times [y_s, y_e] \times [z_s, z_e]$, where $\boldsymbol{x}_s$ and $\boldsymbol{x}_e$ are the coordinates of start and end points respectively. $\boldsymbol{x}_0$ is the mass center of bionic fish. The dimensionless body length of bionic fish is 1. The end condition is $x_0 - x_s \leqslant 1$, where x_0 is the x coordinate of mass center. Therefore, the steps of a fully explicit scheme are shown as following

DO, WHILE $(x_0 - x_s > 1)$

Using the flapping rule, update the body shape of bionic fish at time t;

Using the method of immersed boundary, set the boundary velocity $\boldsymbol{u}_b$ on the surface of fish;

Solving the flow field;

Using the flow field, calculate the hydrodynamic force $\boldsymbol{F}$ and moment $\boldsymbol{M}$;

Using the force $\boldsymbol{F}$ and moment $\boldsymbol{M}$, update the velocities $\boldsymbol{u}$ and $\boldsymbol{\omega}$ of bionic fish;

Using the velocities $\boldsymbol{u}$ and $\boldsymbol{\omega}$, update bionic fish position $\boldsymbol{x}_0$ and orientation $\boldsymbol{\theta}$.

END DO

4. Results and analysis

4.1 The self-propelled swimming of single fish

We now report the result of the self-propelled swimming of single fish. The dimensionless body length(exclude the length of caudal fin) of bionic fish is 1. The computational domain is in the region $6 \times 1 \times 1$. The maximum depth of refinement is 7. The kinematics viscosity coefficient is $\nu = 1.0 \times 10^{-6}$. The Reynolds number based on the length of fish body and the mean velocity of self-propelled swimming. Therefore, the Reynolds number is determined when the simulation is terminated.

Fig.4.1(a) shows that the velocity u is almost the constant. So the fish is in the state of cruise which is the state we will investigated. The velocity v is oscillate in period which leads to the moving path of fish in $x - y$ plan is similar to the shape of "S", as shown in Fig.4.1(c), instead of a straight line. The velocity w is almost zero. As a result, the moving path of fish in $x - z$ plan is a straight line. the movement in z direction is slightly. Fig.4.1(b) shows that the major rotation happens only in $x - y$ plan around z axis. The rotations around other axes can be neglected.

For the mean velocity of self-propelled swimming is $u = 0.46$, the Reynolds number based on the length of fish body is 4.6×10^5. The width of the wake A is often approximated by the lateral total excursion of the end point of peduncle, i.e.

$$A = 2.0(c_1 x_{lp} + c_2 x_{lp}^2) = 2.0 \times 0.155 \times 0.7^2 = 0.152 \tag{4.1}$$

then, the Strouhal number is

$$St = \frac{fA}{u} = \frac{1.0 \times 0.152}{0.46} = 0.33 \tag{4.2}$$

To reveal the vortical structure of the 3D wake, the λ_2 method of Jeong and Hussain[8] is applied to the flow. Fig.4.2 shows the shedding vortical structures of the self-propelled fish. The pressure distribution on the surface is also shown. The generation, shedding, stretching, breakup of the vortical structures can be seen from it. Fig.4.3 shows the adaptive grids in $x - y$ plan($z = 0.0$) and $x - z$ plan($y = 0.0$) at $t = 7.0$. In this study, the maximum depth of refinement is 7. If adaptive grid is not used, the number of total grids is $6 \times 128^3 = 12,582,912$. Forever, the number at $t = 7.0$ is $1,432,050$ now, which is only 11.4% of that without adaptive grid. Therefore, the computational time and memory consuming are decreased greatly.

Fig.4.4 shows the comparison of vortical structures of alive fish(cited from [7]) and our simulation results. Although there are some differences between the shapes of alive fish and the bionic fish, the vortical structures in the wake are similar. From Fig.4.4(a) and (b), it can be seen that both wake are wider and wider from the caudal fin. Fig.4.4 shows the comparison of the wakes of a real fish and a 3D bionic fish, in which the wake picture of the real fish is come from [7]. Although there are difference in the shapes of real fish and a

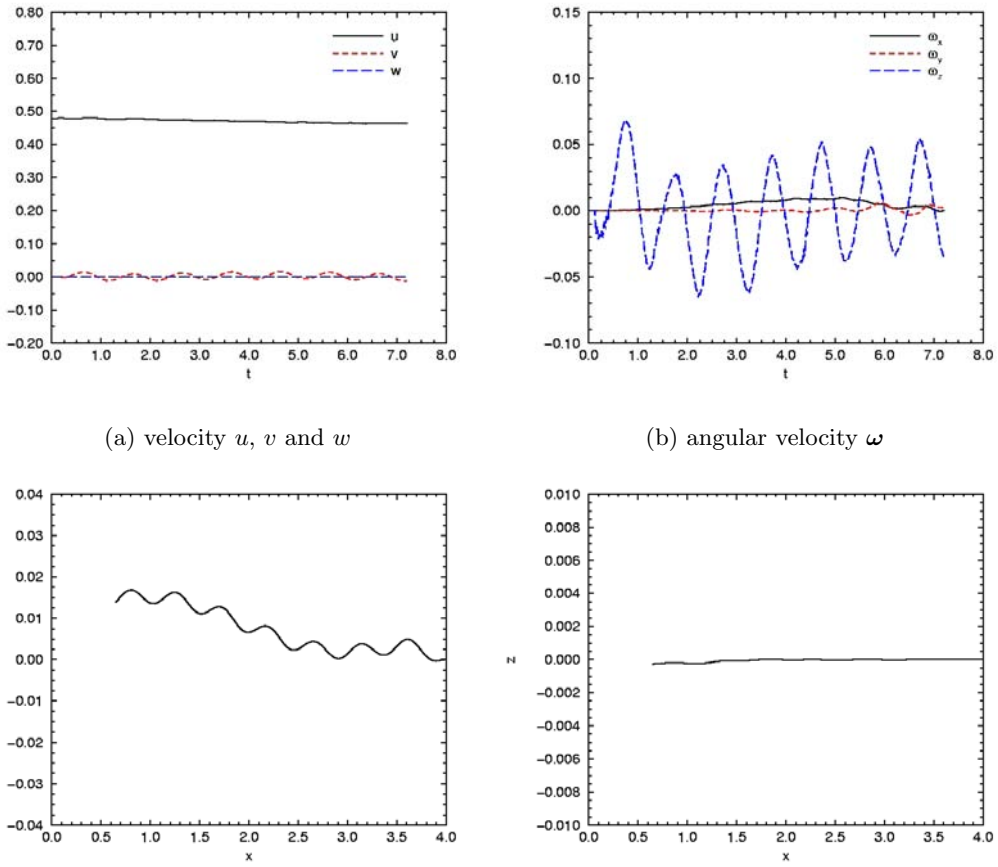

(a) velocity u, v and w

(b) angular velocity $\boldsymbol{\omega}$

(c) the moving path in $x-y$ plan

(d) the moving path in $x-z$ plan

Fig. 4.1 The velocity and moving path of the single fish

3D bionic fish, but their wakes are very similar to each other. From Fig.4.4(c) one can see that in the wake of real fish close to the tail, there are some areas in which vorticity are larger, and from Fig.4.4(d) one can find that in the corresponding area the distribution of vorticity is very similar to the one of real fish.

4.2 Self-propelled swimming of two fish in tandem

Next, the self-propelled swimming of two fish in tandem is investigated. The distance between the mass centers is 1.4 and the flapping phases are in opposite. he computational domain is in the region $6\times1\times1$. The maximum depth of refinement is 7. The fish in the front of the school is called fish-1 and another is called fish-2.

Fig.4.5 shows the velocities and moving path of the self-propelled swimming of tandem fish. Fig.4.5(a) shows the velocity u of fish-2 is smaller than that of fish-1. Fig.4.5(b) shows that the velocity v of fish-1 is almost zero, while the v of fish-2 becomes $v<0$. Fig.4.5 shows the velocity and path of self-propelled swimming of 3D bionic fish in tandem. From Fig.4.5(a) it is seen that the u of fish 2 is obvious smaller than that of fish 1. From Fig.4.5(b) one can find that the v of fish 1 is essentially symmetrical about $v=0$, but the v of fish 2 gradually deflects to the side where $v<0$. Therefore, from the path in Fig.4.5(d) it is seen that fish 1 on the whole keeps moving in straight line, but the path of fish 2 gradually diverges, with the maximum offset equals to 0.034. Because of the deflection of the path which causes the decrease of u, this is very similar compared to the situation in 2D cases. From Fig.4.5(d), we see that the w of two fish are essentially zero, therefore there will be no deflection in the z direction.

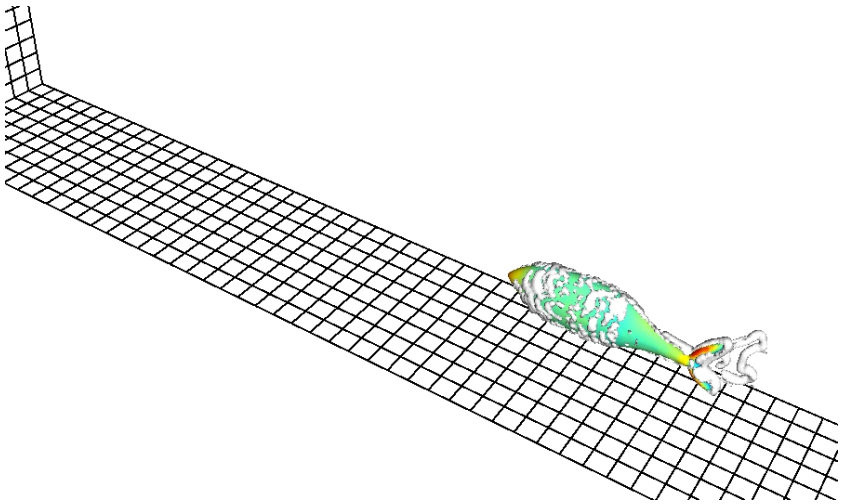

(a) $t = 0.50$

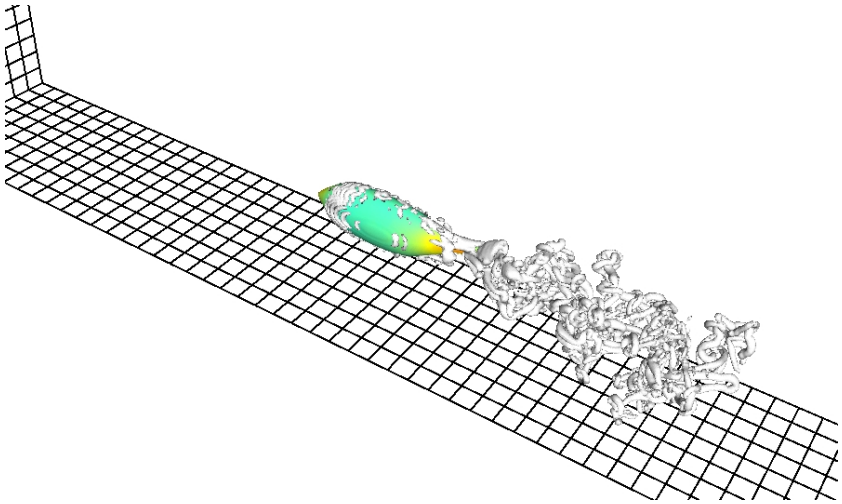

(b) $t = 3.00$

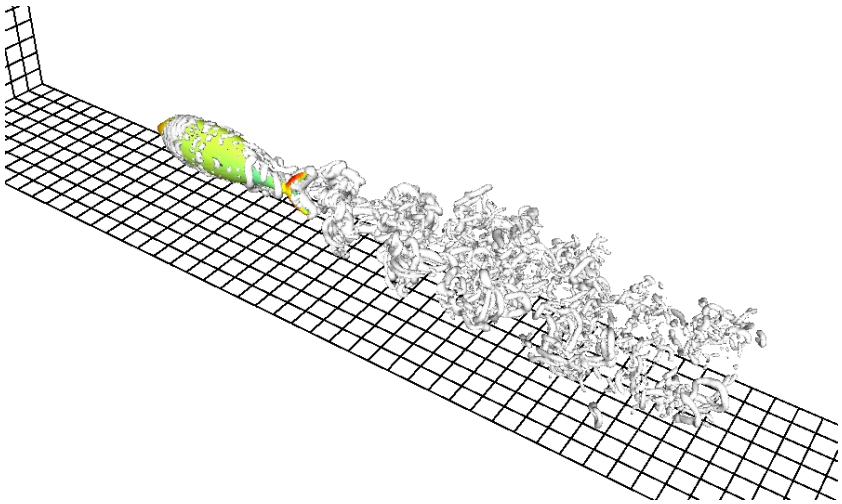

(c) $t = 5.50$

Fig. 4.2 The shedding vortical structures of the self-propelled swimming of single fish(the color on the body surface represents the pressure)

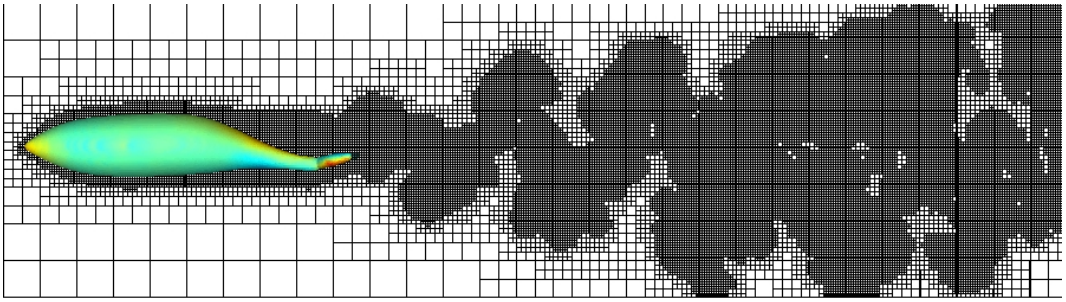

$x-y$ section($z=0.0$)

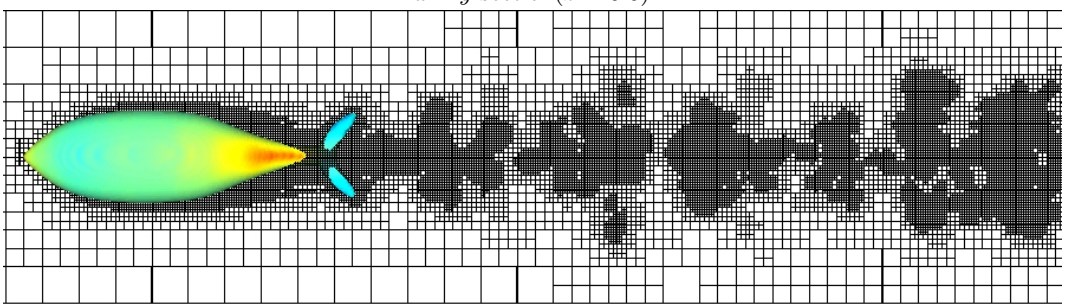

$x-z$ section($y=0.0$)

Fig. 4.3 The adaptive grid of self-propelled fish($t=7.0$, the color on the body surface indicates the pressure distribution.)

Fig.4.6 shows the wake of two self-propelled swimming 3D bionic fish in tandem, shown in the iso-surface of λ_2. For the results of the fluid mechanics and control mechanism will be given in other papers.

(a) The wake of a fish (1)

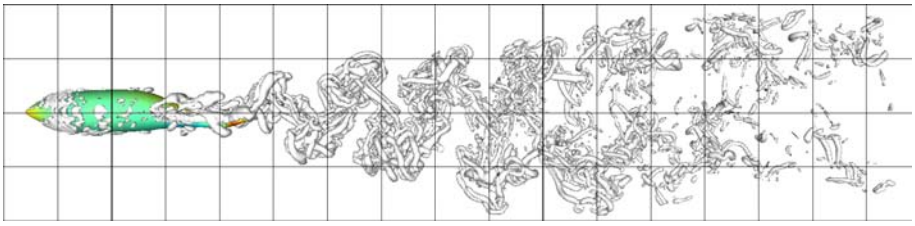

(b) The 3D iso-surface of λ_2 observed from above at $t = 7.0$(the color on the body surface indicates the pressure distribution)

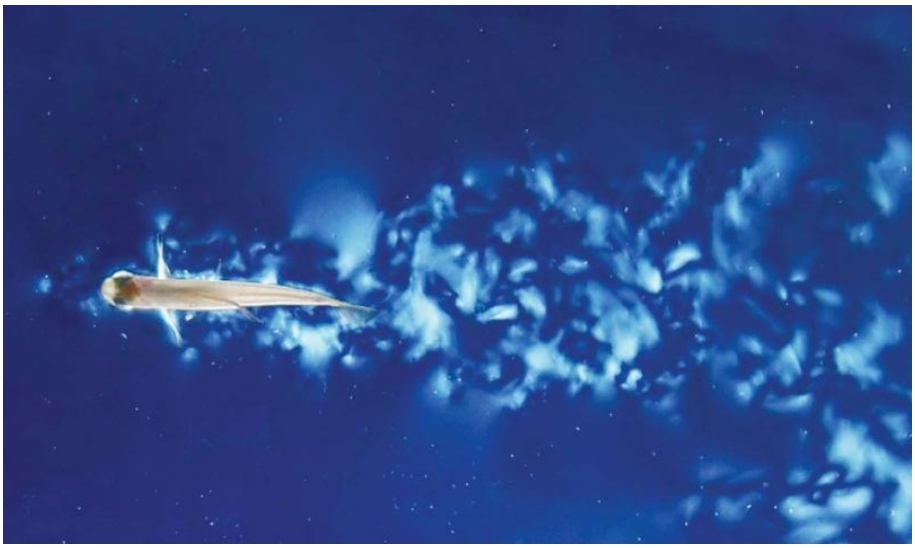

(c) The wake of a fish (2)

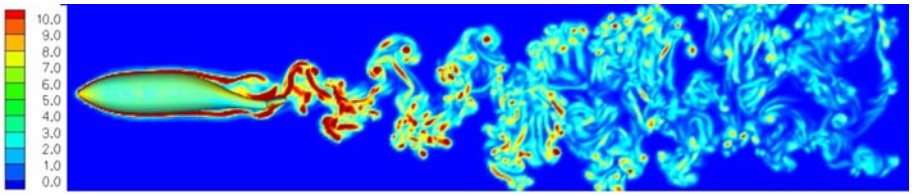

(d) The total vorticity distribution at $t = 7.00$ and $x - y$ section($z = 0.0$)(the color on the body surface indicates the pressure distribution)

Fig. 4.4 The comparison of wakes of a fish and a 3D bionic fish

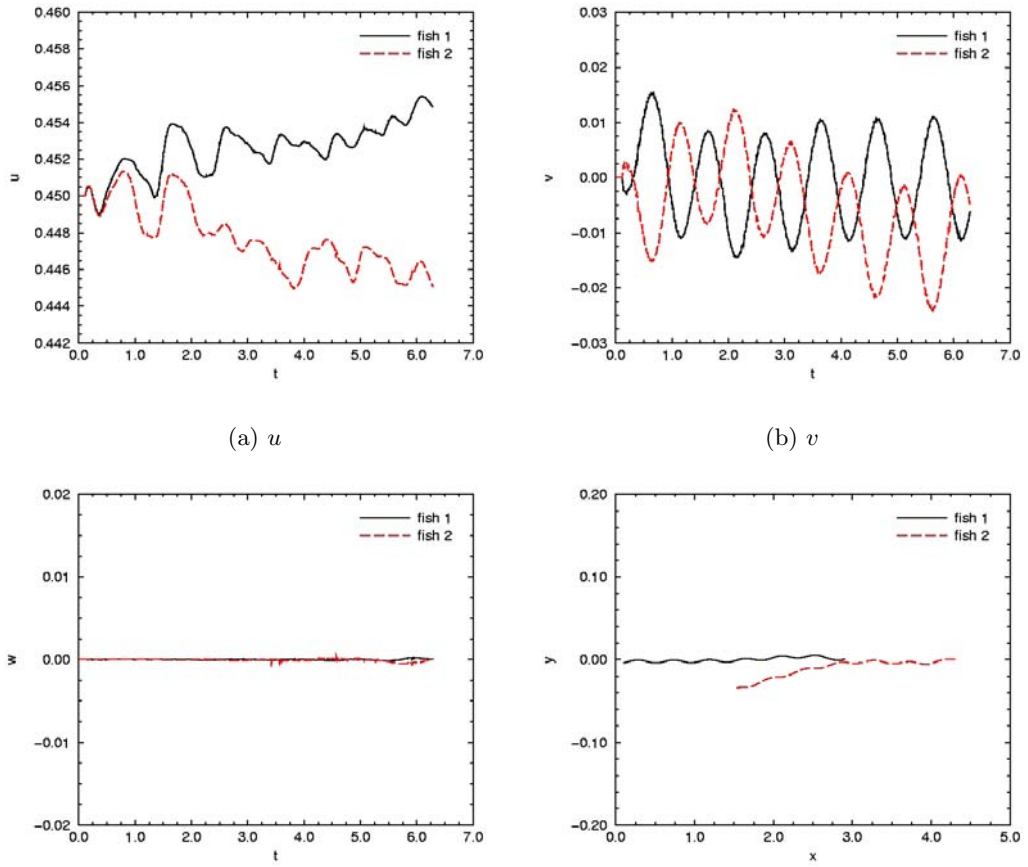

(a) u (b) v

(c) w (d) The projection of path in $x-y$ plan

Fig. 4.5 Velocities and moving path of the self-propelled swimming of fish in tandem.

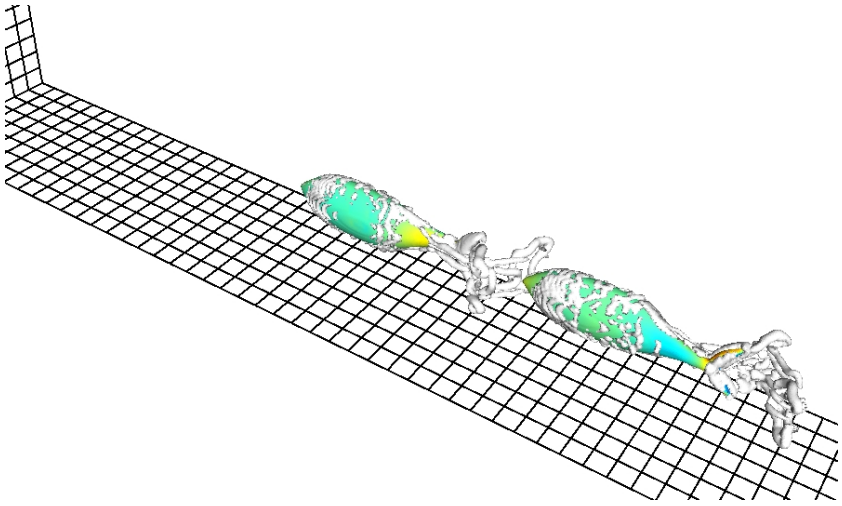

(a) $t = 1.00$

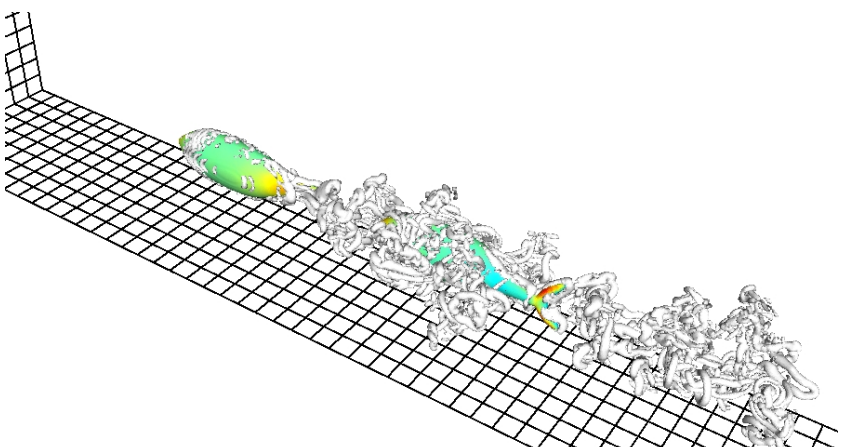

5. Conclusions

From the study of the self-propelled swimming of 3D bionic fish school in a viscous fluid in a tank, we arrive following conclusions:

1. The parallel numerical algorithm and codes for the 2D and 3D moving boundary problem is obtained, which combines the adaptive multi-grid finite volume method and the methods of immersed boundary and VOF (Volume of Fluid). The reliability of the algorithm and code is verified with the numerical results of flow around a 2D circular cylinder;

2. Using above numerical algorithm and codes, the self-propelled swimming of 3D bionic fish school in a viscous fluid is got for the first time;

3. In the self-propelled swimming of a 3D bionic fish, vortices are shed off from the area close to the narrow peduncle, at which the caudal fin attaches to the trunk. The phase of shedding vortices is opposite to that of flapping tail. Vortices shed from trunk merge with the vortices with the same rotating direction, induced by the caudal fin. As a consequence, the efficiency of propulsion is increased.

4. Without control, when two 3D bionic fish swimming in tandem, the rear one's path will deflect under the influence of the vortices shed from the front one.

References

1. Bell, J. B., Colella, P. & Glaz, H. M., A second-order projection method for the incompressible Navier Stokes equations, *J. Comput. Phys.*, 1989, **85**: 257-283.
2. Gueyffier, D., Li, J., Nadim, A. & Scardovelli, R., Volume-of-Fluid Interface Tracking with Smoothed Surface Stress Methods for Three-Dimensional Flows, *J. Comput. Phys.*, 1999, **152**(2): 423-456.
3. Khokhlov, A.M., Fully threaded tree algorithms for adaptive refinement fluid dynamics simulations, *J. Comput. Phys.*, 1998, **143**(2):519-543.
4. Popinet, S., Gerris: a tree-based adaptive solver for the incompressible Euler equations in complex geometries, *Journal of Computational Physics*, 2003, **190**:572-600.
5. Chang, I-C, Torres, F. J. & van Dam, C. P., 1991, Wing design code using three-dimensional Euler equations and optimization, *AIAA 91-3190*.
6. Dias, A. & Majumdar, S., *Numerical computation of flow around a circular cylinder*, Technical Report, PS II Report, BITS Pilani, India.
7. David, L. H., Lucy, M., Brian, C., Thomas, G. & John, W. M., 2005, Visualization of a fish wake using tobacco mosaic virus, *J. Phy. of Fluids*, **17**, 091103.
8. Jeong, J. & Hussain, F., 1995, On the identification of a vortex. *J. Fluid Mech.*, **285**:69-94.
9. Kim, J., Kim, D. & Choi, H., 2001, An immersed-boundary finite-volume method for simulations of flow in complex geometries, *J. Comput. Phys.*, **171**:132-150.
10. Lai, M. & Peskin, C. S., 2000, An immersed boundary method with formal second-order accuracy and reduced numerical viscosity, *J. Comput. Phys.*, **160**:705-719.
11. Tseng, Y. H. & Ferziger, J. H., 2003, A ghost-cell immersed boundary method for flow in complex geometry, *J. Comput. Phys.*, **192**: 593-623.
12. Wolfgang, M., Anderson, J. M., Grosenbaugh, M. A., Yue, D. K. P. & Triantafyllou, M. S., 1999, Nearbody flow dynamics in swimming fish, *J. Exp. Biol.*, **202**:2303-2327。
13. Zdravkovich, M. M., 1997, *Flow Around Circular Cylinders. Vol. 1: Fundamentals*, Oxford University Press, New York.
14. Zhu, Q., Wolfgang, M. J., Yue, D. K. P. & Triantafyllou, M. S., 2002, Three-dimensional flow structure and vorticity control in fish-like swimming, *J. Fluids Mech.*, **468**:1-28.